Journal of Structural Geology 32 (2010) 1250–1256

Contents lists available at ScienceDirect

Journal of Structural Geology

journal homepage: www.elsevier.com/locate/jsg

Stylolites in limestone: Magnitude of contractional strain accommodated and scaling relationships

Antonio Benedicto [a,*,1], Richard A. Schultz [b]

[a] Laboratoire de tectonique, CNRS/INSU UMR-7072 Tectonique, Université Paris XI, 91405 Orsay, France
[b] Department of Geological Sciences and Engineering, University of Nevada, Reno, NV 89557, USA

ARTICLE INFO

Article history:
Received 23 November 2007
Received in revised form
14 August 2008
Accepted 9 April 2009
Available online 21 May 2009

Keywords:
Stylolite
Growth
Scaling
Faulting
Limestones
Pressure-solution

ABSTRACT

The amount of contractional strain accommodated by a set of stylolites is analyzed by comparing the amplitudes of stylolitic teeth and spikes to independent measures of thinning of the enclosing layer. The scaling relations between along-strike trace length (L) and the maximum (D_{max}) and average (D_{avg}) amplitudes of stylolitic topography are also investigated. The studied stylolites occur in a 212-mm thick limestone layer dragged into the damage zone of the Gubbio normal fault zone in central Italy. Layer thinning was assessed independently from the layer geometry, with a maximum value of ~23% nearest the fault. A total of 28 mm of thinning are related to 24 stylolites whose lengths range from 6.4 to 146 mm with average amplitudes from 0.1 to 1.3 mm. The average and maximum amplitudes of stylolitic topography increase with stylolite length, with $D_{avg} = 0.0011L^{0.17}$, $r^2 = 0.57$, implying propagation to greater lengths as contractional strains increase along them. The stylolites increase in number and amplitude into the most thinned area, correlating with increasing contractional strain accommodated by the layer. The average amplitude of stylolites visible in outcrop provides a measure of the minimum magnitude of contractional strain in the rock, although other mechanisms such as grain-scale dissolution appear necessary to account for the remaining layer thinning.

1. Introduction and background

Stylolites are distinctive and pervasive structures that result from water-assisted pressure solution in rocks such as limestones and dolomites (Rutter, 1983; Passchier and Trouw, 1996). The orientations of stylolite surfaces and the associated topography (spikes and teeth) track the direction of the local stress state (e.g. Suppe, 1985; Petit and Mattauer, 1995), making them reliable paleostress indicators (Stel and De Ruig, 1989; Koehn et al., 2007) comparable to anticracks (Fletcher and Pollard, 1981) and compaction bands (Holcomb et al., 2007).

Stylolites are thought to be analogous mechanically to anti-cracks (Fletcher and Pollard, 1981; Rispoli, 1981a,b; Tapp and Cook, 1988) that propagate to greater lengths (Tapp and Cook, 1988; Carrio-Schaffhausen et al., 1990) as contractional strains increase along them, similar to compaction bands in porous sandstones (Mollema and Antonellini, 1996; Sternlof et al., 2005; Katsman and Aharonov, 2006; Katsman et al., 2006; Schultz, 2009). Stylolites nucleate at local heterogeneities in the rock, such as grains of differing rates of dissolution, mica flakes, or other small-scale physical or chemical perturbations. When stylolites start to grow (called micro-stylolites), peaks develop in a regime in which there is a competition between the effect of strain energy that promotes the peak development and surface energy ("capillary" forces) that limits it (Renard et al., 2004; Brouste et al., 2007; Koehn et al., 2007). The result is that stylolites develop with relatively smaller amplitudes at small sizes (producing flat stylolites at outcrop scale) than at larger sizes. Once a stylolite's length L becomes sufficiently large relative to the average grain size l of the rock, however (i.e., a cross-over length $L/l > 10$–100; see Renard et al., 2004; Brouste et al., 2007; Koehn et al., 2007), then amplitude increases with contractional strain. As a result, stylolites record a variable minimum value of the actual magnitude of contractional strain in the rock and a scaling relationship between stylolites topography (amplitude) and length is expected.

The minimum magnitude of contractional strain accommodated by a stylolite has been difficult to assess given the dependence of the amplitude of peaks on the properties and chemical heterogeneity of the surrounding rock (Brouste et al., 2007; Koehn et al., 2007). Effectively, stylolitization is a complex self-organized

* Corresponding author. Tel.: +33 1 34 96 37 10.
E-mail address: antonio.benedicto@areva.com (A. Benedicto).
[1] Present address: Areva NC, BU Mines, Direction des Géosciences, Tour Areva, BAL520A, 1 Pl. Jean Millier, 92094 Paris La Défense Cedex, France.

0191-8141/$ – see front matter © 2009 Published by Elsevier Ltd.
doi:10.1016/j.jsg.2009.04.020

system in which the passive concentration of insoluble species progressively changes both the kinetics and the geometry of the stylolites with time. For example, the amplitudes of spikes and teeth associated with water-assisted diffusive mass loss across a stylolite increase with the number and density of less soluble phases (Renard and Dysthe, 2003; Koehn et al., 2007). But on the other hand, mica concentration can enhance pressure solution and passive concentration of insoluble minerals can progressively flatten the stylolites (J.P. Gratier, *personn. comm.*). Koehn et al. (2007) show how the roughening of stylolites passes from a regime of power-law growth through a regime where the roughness potentially saturates. Ultimately an increase of contractional strain can lead to a decrease of the rate of increase of the rate of increase of the peak amplitude of the stylolites.

Taking into account the previous considerations, it could be expected that a population of sufficiently large stylolites (large in order to avoid the influence of "capillary" should give a minimum value of the accommodated strain. Here, we calculate this minimum value in such a population of stylolites. We analyse well-constrained fault-related stylolites within micritic limestones in order to: (1) quantify the magnitude of the contractional strain accommodated across the stylolites by comparing the amplitudes of stylolitic teeth and spikes to independent measures of layer thinning; and (2) investigate the scaling relations between along-strike trace length (L) and both maximum (D_{max}) and average (D_{avg}) amplitudes of stylolitic topography. Calculations of the minimum accommodated strain by natural stylolites, in addition to numerical modelling, are necessary to better understand the process of dissolution and mass lost under tectonic strain.

2. Study area and block

The study area is located along the Gubbio normal fault in central Italy (Fig. 1a). This fault is 22 km long, with ~3200 m of displacement near its midpoint, and is seismically active (Boschi et al., 1997; Boncio et al., 2000). The fault strikes NW–SE, dips to the SW, and juxtaposes Mesozoic marine limestones, in the footwall, against Plio-Quaternary lacustrine sediments, in the hangingwall (e.g. Menichetti and Minelli, 1991; Collettini et al., 2003). The study block is located in the western cliff face of the Cava Filippi quarry

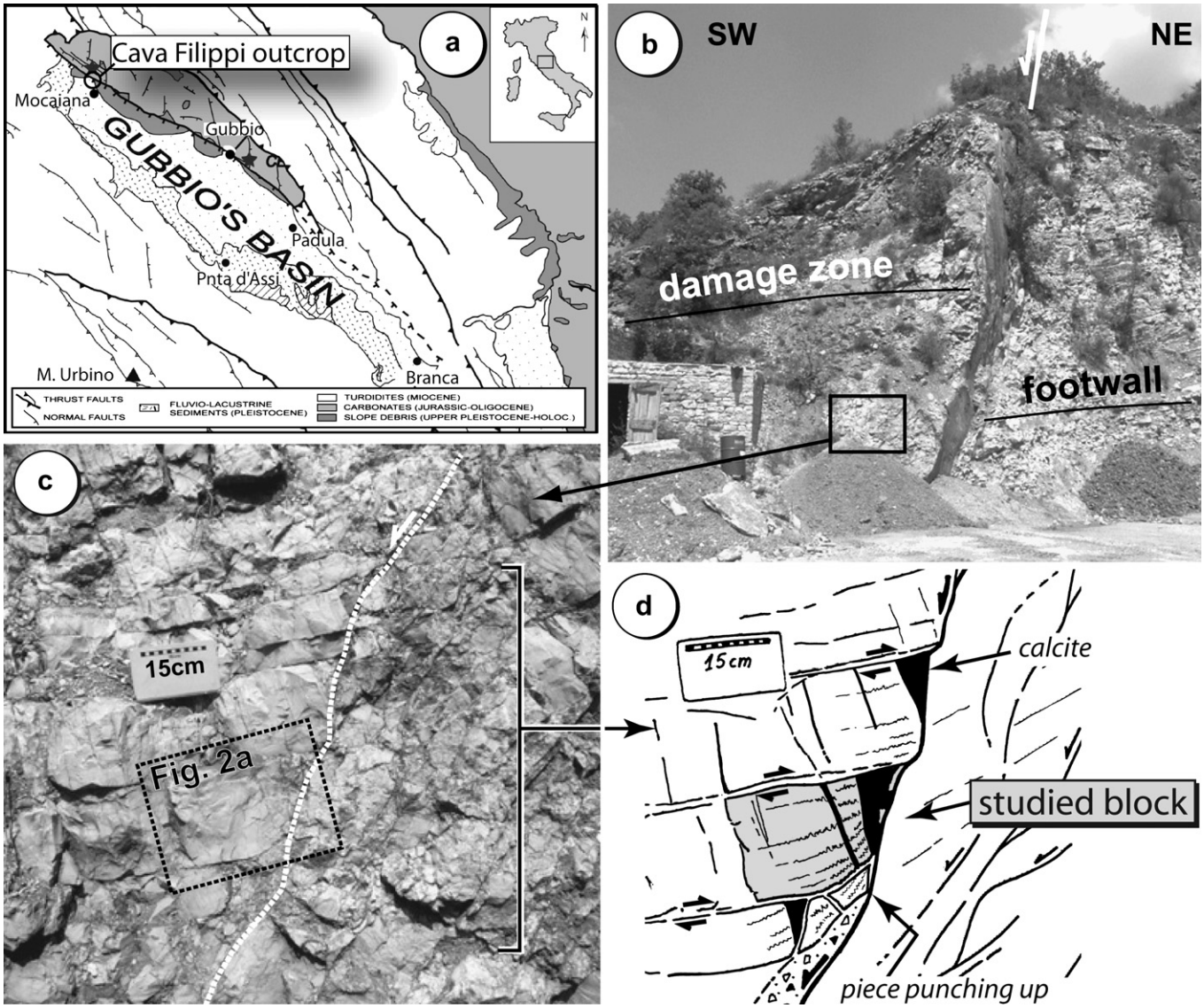

Fig. 1. Study area and block. a) Location of the Gubbio fault. b) and c) Location of the studied block and magnified view. d) Sketch showing the main structural elements of the studied block and surrounding areas.

which traverses the entire fault zone near its northwestern tip (Fig. 1b). The structure of the fault zone in this quarry is described in Bussolotto et al. (2005, 2007).

The block studied (Fig. 1c) is situated in the inner domain of the fault's damage zone, approximately two meters away from the main fault that separates the non-deformed footwall from the fault damage zone (Fig. 1c). This faulted domain involves fine-grained mudstone layers of the reddish marly calcareous *Scaglia rossa Fm.* (Coniacian-Upper Paleocene) which are here highly fractured and tilted, but still well recognizable. The block is part of a limestone layer that was thinned during normal faulting (Fig. 1d), comparable to the deformation sequence observed by Micarelli et al. (2005) along the La Remuque fault in southern France. Layer thinning was accompanied by stylolite growth in both cases, and was enhanced in the studied block by the punching effect of a piece of the subjacent layer that remained locked on a restraining bend of the fault during displacement of the hangingwall (Fig. 1d). Bending of the layer inducing stylolite growth was also accommodated by cracking and calcite vein growth. The kinematics suggests that layer thinning was greater near the fault (right-hand side of Fig. 1d) and decreased to a negligibly small value beyond ~2 m away (left-hand side of Fig. 1d).

3. Approach

The studied block of 20 × 20 cm in size (Fig. 2a) was divided into 4 areas (A, B, C and D) of increasing block thinning (Fig. 2b). Area A corresponds to the undeformed part of the layer. It only contains the tips of two stylolites (S6, S24). Although the irregular morphology of the lower and upper contacts of the layer beyond Area A suggests pressure solution related to post-depositional compaction, the lack of stylolites within the same layer, farther away from the fault, indicates the initial layer thickness before faulting and stylolite growth (after compaction). We incorporate this uncertainty concerning layer thickness into the analysis below. Area B corresponds to the flat portion of the layer where stylolites start to appear. Areas C and D correspond to the thinned and rotated portion of the layer approaching the fault, separated by a calcite vein that is orthogonal to bedding.

We identified sedimentary markers, consisting in fine micrite laminae both at the base and the top of the limestone layer, which did not appear to have been disturbed by dissolution. They define the shape of the thinned layer. The amount of thinning was calculated by using these markers with $\epsilon_{layer} = \Delta T/T_0$, where ΔT is the reduction in layer thickness from the initial value $T_0 = 212.4$ mm measured far from the fault, in Area A, where no significant stylolites occur. Data obtained from this block are listed in Table 1.

The amplitudes of the stylolitic topography were measured along the lengths of the selected stylolites from enlarged digital images of the study block. The morphology of the fine indented peaks was simplified for measurement as depicted in the inset sketch in Fig. 2c. Following the simulation results of Koehn et al. (2007), we then constructed an envelope of the amplitude of the stylolitic topography in the limestone block as an estimate of area lost across the stylolite (Fig. 2c, inset). Lengths were measured along the curving trace of the stylolite, with amplitudes measured incrementally along the length given by the width of the envelope perpendicular to the stylolite's local orientation.

The total contractional strain, accommodated by the measured stylolites in the block, can be calculated by summing the contributions of each stylolite and dividing this sum by the original (undeformed) area of the layer. This approach, used extensively in seismotectonics and structural geology (e.g. see Aki and Richards, 1980, pp. 117–118; Molnar, 1983; Scholz and Cowie, 1990; Westaway, 1992; Scholz, 1997; Scholz, 2002, pp. 306–309; Wilkins et al., 2002; Schultz, 2003), is given by Kostrov's (1974) formula as

$$\epsilon = \frac{1}{A_0}\sum_{i=1}^{N} D_i L_i \qquad (1)$$

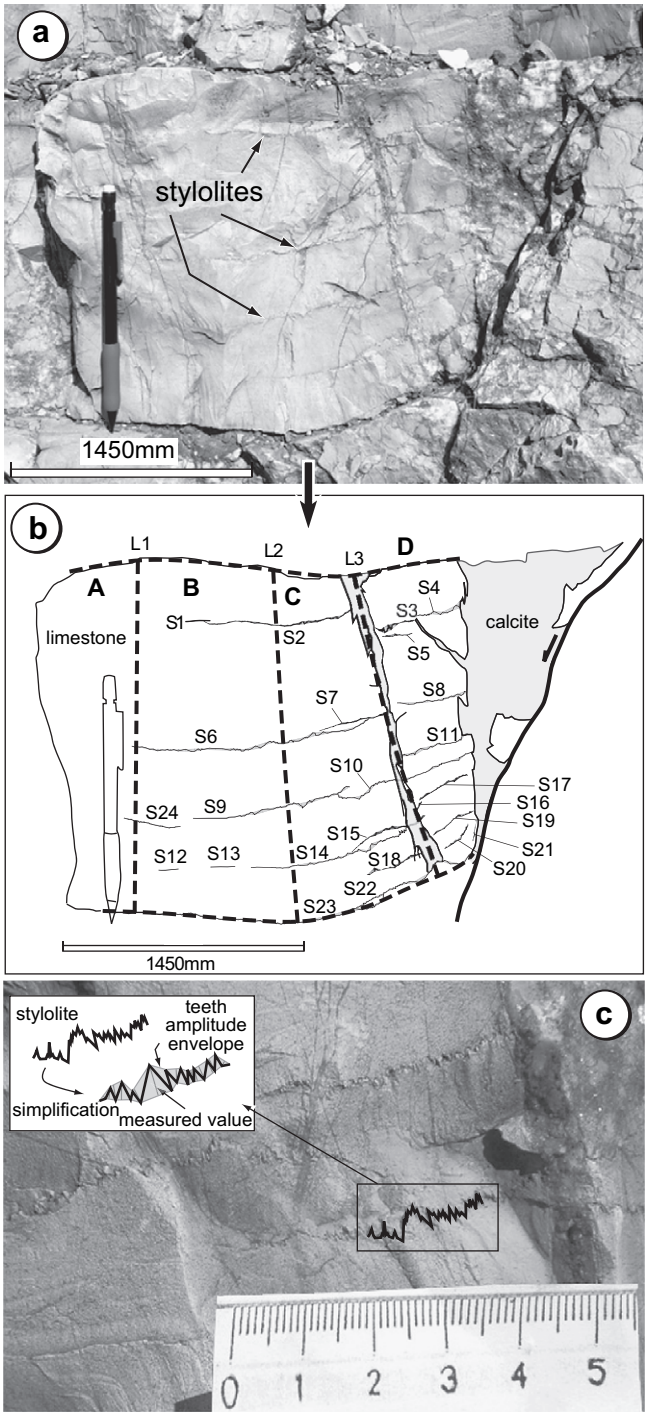

Fig. 2. a) Studied block with stylolites. b) Sketch depicting the stylolites and the areas of different layer thinning and increasing strain in which the block was divided for this study (A, B, C, D); a strand of the Gubbio fault forms the right-hand side of the deformed layer (see Fig. 1). c) Measurement technique for an individual stylolite.

Table 1
Dimensions of block domains.

Domain	Description	T, mm	A, mm^2
A	Few stylolites	212.4	5,720.017
B	Several stylolites	212.0	10,788.571
C	Many stylolites	193.9	8,189.259
D	Between calcite veins	162.3	5,406.728

All blocks assume original thickness $T_0 = 212.4$ mm with measurement uncertainties of ± 0.5 mm.

in which D_i is the average amplitude, L_i is stylolite length, and A_0 is the original cross-sectional area (A–D) of the deformed block. In this paper we use this approach noting that the expression in Eq. (1) is sufficiently general to provide values for normal strain from the lengths and inferred closing displacements of stylolites. The average amplitude for a given stylolite was calculated from the maximum values of its envelope. Only the stylolites visible on the outcrop photograph (Fig. 2b) were measured, in consequence the values of total contractional strain calculated using Eq. (1) represent minimum (or lower) values of the total shortening accommodated by pressure solution in the layer. Cross-sectional areas of each part of the block (A–D) were calculated from digitized maps of their shapes (Table 1). Block areas are uncertain due to exposure to perhaps $\pm 5\%$, whereas the calculated stylolite strains are uncertain to perhaps $\pm 20\%$ of their values.

4. Morphology of the stylolites

A total of 24 stylolites were identified and measured (Fig. 3). Lengths and maximum amplitudes of stylolitic topography range from 6 to 146 mm and 0.2 to 3.7 mm, respectively (Table 2). The stylolites change systematically from surfaces of negligible to small topography in areas A and B to higher-amplitude structures in areas C and D (Fig. 3). The sudden increase in the average and maximum amplitudes of stylolitic topography corresponds to the location of significant bending of the layer (area C). The number of stylolites also increases progressively from area A to area D, i.e. towards the fault.

The envelopes of stylolitic topography exhibit three distinct morphologies. Many stylolites are asymmetric, with the amplitude of topography increasing progressively and systematically from a minimum at either tip to a maximum value located away from the midpoint of the stylolite (orange and purple stylolites in Fig. 3). Only three stylolites show symmetric envelopes with the maximum values located at or near the stylolites' midpoints (yellow stylolites in Fig. 3); three others show a composite shape with two peaks of maximum values distributed arbitrarily along the stylolite (blue stylolites in Fig. 3).

The dominant shape of the stylolites longer than 2 cm is right-asymmetric (Fig. 3), with average and maximum amplitudes skewed towards the fault. Stylolites with this shape are the longest and go from areas D or C through areas B and A. Their profiles

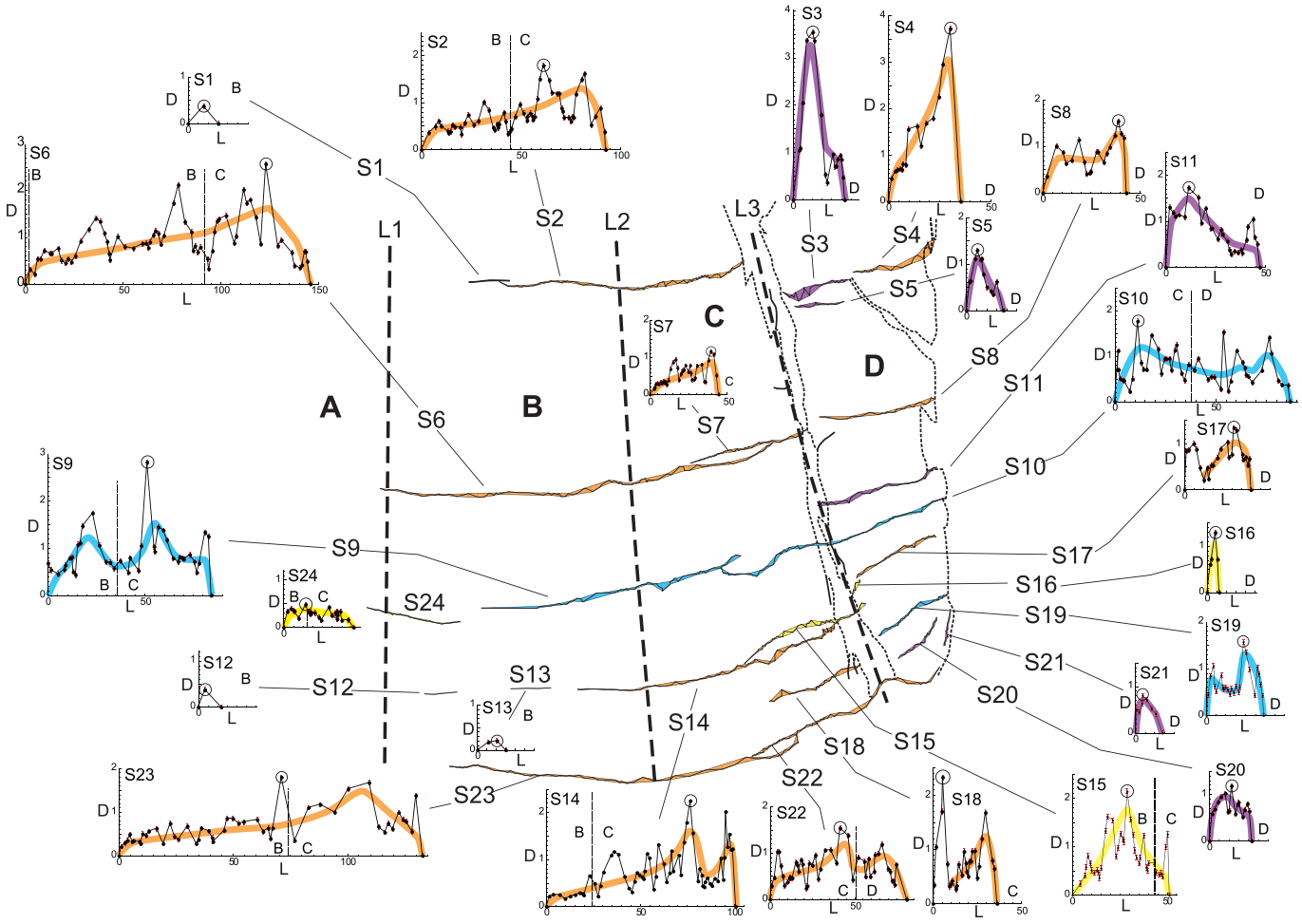

Fig. 3. Map of stylolites and plots of amplitude versus length for each stylolite measured.

Table 2
Dimensions of stylolites.

Stylolite	Total length, mm	D_{avg}, mm	D_{max}, mm	D_{avg}/L	D_{max}/L
S1	15.29	0.126	0.377	0.00824	0.0247
S2	92.53	0.715	1.791	0.00773	0.0194
S3	26.88	1.260	3.543	0.0469	0.132
S4	35.58	1.272	3.727	0.0358	0.105
S5	18.20	0.656	1.300	0.0360	0.0714
S6	145.89	0.931	2.568	0.00638	0.0176
S7	44.43	0.514	1.165	0.0116	0.0262
S8	43.184	0.769	1.536	0.0178	0.0356
S9	84.253	0.885	2.814	0.0105	0.0334
S10	86.622	0.726	1.772	0.00838	0.0205
S11	47.086	0.766	1.729	0.0163	0.0367
S12	11.904	0.125	0.374	0.0105	0.0314
S13	15.068	0.095	0.204	0.00630	0.0171
S14	100.8	0.738	2.252	0.00732	0.0223
S15	51.01	0.797	2.145	0.0156	0.0421
S16	6.393	0.554	1.291	0.0867	0.202
S17	34.808	0.668	1.339	0.0192	0.0385
S18	36.209	0.746	2.327	0.0206	0.0643
S19	29.204	0.664	1.57	0.0227	0.0538
S20	21.661	0.670	1.183	0.0309	0.0546
S21	14.03	0.451	0.807	0.0322	0.0575
S22	80.946	0.669	1.540	0.00826	0.0190
S23	132.863	0.635	1.795	0.00478	0.0135
S24	36.087	0.268	0.486	0.00743	0.0135

exhibit a progressive increase of the average of the amplitude with the length, or inversely, a decreasing amplitude when moving from area D to A, consistent with the progressive layer thinning and increasing contractional strain with increasing distance from the fault (discussed below). This suggests that the stylolites nucleated first in the part of the block nearest the fault (area D) and propagated away from the fault (into areas C, B, and A) as their amplitudes and the amount of layer thinning increased.

Left-asymmetric, symmetric and composite stylolites are shorter than the more common right-asymmetric stylolites described above, and they mainly occur in the most thinned part of the block (area D). Their profiles suggest that in this area the strain was distributed homogeneously, probably due to the confinement of this area between two calcite-filled fractures, with the direction of stylolite propagation in this area freely from right to left and/or inversely.

5. Amount of layer thinning

Using the approach outlined above, the layer thickness decreases progressively from its initial thickness of $T_0 = 212.4$ mm to a minimum of 162.3 mm, adjacent to the fault. This corresponds to a contractional (bedding-normal) normal strain of about 23.6% (Table 3, Fig. 4, open symbols). Layer thinning appears to have been accompanied by a counterclockwise rotation of the parts of the layer nearest the fault (Fig. 2); the stylolites also mirror this rotation, suggesting that they formed at an early stage, before significant layer rotation occurred or synchronously.

By summing lengths and average amplitudes using Kostrov's formula, the contractional strain accommodated by the stylolites increases from zero far from the fault (in area A) to ~5% in the area of greatest layer thinning (area D; Fig. 4, filled symbols). Although the amount of layer thinning and contractional strain accommodated by the stylolites both increase towards the fault (from area A to area D), the rates of increase are not the same, as shown by the ratios of stylolite strain to block strain (Table 3). Nearest the fault, in area D, the amount of contractional strain associated with layer thinning was ~20 times that measured from the stylolites' amplitudes. As the value of the contractional strain measured from stylolites' amplitude is only a minimum value of the accommodated strain (as mentioned above in the Introduction and Background Section), this means that stylolites account for about one-fifth of the material lost from the layer as it thinned.

Table 3
Contractional strains of block domains.

Domain	Description	Block strain, %	Stylolite strains, %	Stylolite/Block, %
A	Few stylolites	0.0	0.47	–
B	Several stylolites	0.19	1.93	1026.5
C	Many stylolites	8.7	4.54	52.2
D	Between calcite veins	23.6	4.72	20.0

6. Displacement–length scaling relations

Two types of displacement–length (D–L) profiles were analyzed from a subset of the mapped envelopes of stylolitic topography: D_{max}/L and D_{avg}/L profiles, in which L is the length and D_{max} is the maximum amplitude of the stylolitic topography, and D_{avg} is its average amplitude. D corresponds, in either case, to the measured displacement of host rock across the plane of the stylolite. Displacement is considered in a closing or contractional sense with attendant removal by dissolution, as in the case of anticracks. Of the 24 stylolites measured, only 18 of these exhibited clear and sufficiently detailed profiles that permitted confident identification of their maximum or average displacements. The stylolites not plotted are: S1, S3, S4, S12, S13, and S20.

Log-log plots of maximum amplitude versus length show an increase with stylolite length (Fig. 5), with $D_{max} = 0.0038L^{0.29}$ $r^2 = 0.68$. The slope of ~0.3 is smaller than that associated with other datasets for anticracks available in literature, those of compaction bands from sandstone in the Valley of Fire, southern Nevada, and in southern Utah, which have a slope close to 0.5 (Sternlof et al., 2005; Holcomb et al., 2007; Schultz, 2009). The envelopes of stylolitic topography (e.g. Fig. 4, inset) show, however, that peaks having the maximum amplitude can occur anywhere along the stylolite, even close to a flat tip (e.g. stylolite S14; see also the results shown by Koehn et al., 2007). Furthermore, in the most thinned parts of the layer (areas C and D), spikes of shorter stylolites can have anomalously large amplitudes (e.g. stylolites S3 or S4, with $D_{max} > 3$ mm) compared to those of shorter stylolites in areas A andB (e.g. stylolites S13 or S24, with $D_{max} < 1$ mm).

These nonsystematic variations in the locations of peaks (and hence D_{max}) cause significant modifications of the D_{max}/L profiles and hinder the identification of displacement gradients along the stylolite. The scaling relations that use D_{max} are consequently inconsistent. This is in agreement with Koehn et al. (2007), who suggest that the amplitude of stylolitic topography depends on where the less soluble particles in the host rock are in relation with the developing stylolite surface. This relationship implies that the local chemical heterogeneities of the host rock have more influence on the maximum amplitude (and its location along the lengthening stylolite) than the magnitude of the contractional strain.

In contrast, the average displacements along a stylolite provide a truer representation of the shape of the stylolitic surface, and therefore of the amount of volume loss and contractional strain it has accommodated. The relationship between the average of the amplitude, D_{avg}, calculated from the envelope of stylolitic topography, and the length of the stylolite, is found to be $D_{avg} = 0.00111L^{0.17}$, $r^2 = 0.57$ (Fig. 5). This scaling relationship neglects the effect of host rock heterogeneities at the grain scale and better reflects the average mechanical response of the host

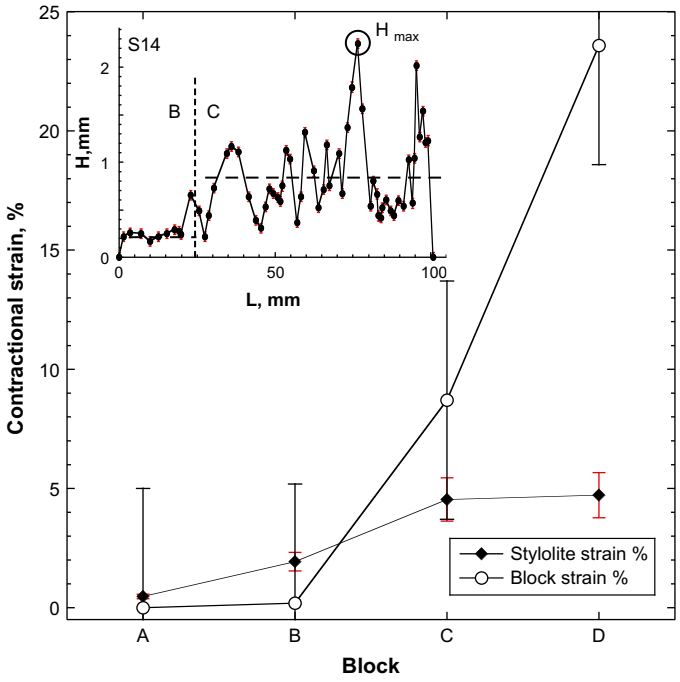

Fig. 4. Plot of contractional strain accommodated by layer thinning (open symbols) and stylolites (filled symbols) versus proximity to the fault (right side); uncertainties as noted in text. Inset shows calculated values of the maximum and average amplitudes of the stylolitic topography within the block.

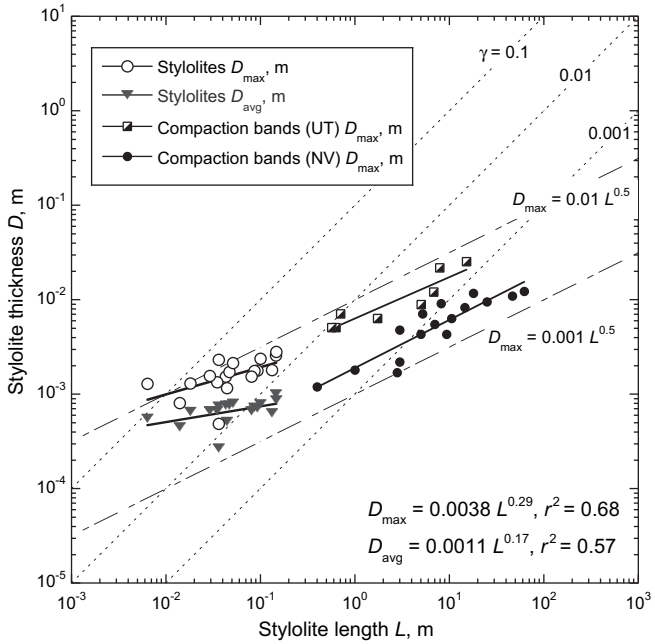

Fig. 5. Stylolite thickness–length (displacement–length) scaling relations for 18 Gubbio stylolites. For comparison, data for compaction bands is plotted (NV bands, Sternlof et al., 2005; UT, Schultz, 2009). Lines of constant slope are shown: $n = 1$, dotted, characteristic of faults; $D/L = \gamma$, $n = 0.5$, dashed, characteristic of anticracks and compaction bands.

rock to localized dissolution along the stylolitic surfaces. Average displacements are commonly used in studies of the crustal strains accommodated by faulting, e.g. Scholz and Cowie (1990).

The mild dependence of average amplitude on stylolite length (i.e. the scaling exponent of 0.17) indicates that topography, and hence contractional strain, increase with stylolite length. As demonstrated by Olson (2003) and others, a scaling exponent of 0.5 indicates fracture growth under conditions of constant fracture toughness, whereas an exponent of 1.0, typical of faults (e.g. Clark and Cox, 1996; Schultz et al., 2008) indicates growth under conditions of constant driving stress. The scaling exponent for the Gubbio stylolites of 0.17 indicates a faster increase in length relative to stylolitic topography, perhaps implying that a near-tip stress amplification (e.g. Fletcher and Pollard, 1981; Tapp and Cook, 1988; Carrio-Schaffhausen et al., 1990) facilitates dissolution of the host rock there.

The asymmetric shape of the longest stylolites indicates propagation of the stylolites from the more thinned to the less thinned parts of the layer. In that sense, it is interesting to note that the sense of asymmetry of stylolitic topography could be related to propagation of the stylolites with increasing strain, while the irregularly positioned maxima are related to the physical or chemical heterogeneities in the rock that are intercepted by the stylolites during their lateral propagation, consistent with Brouste et al. (2007). This suggests that the D_{avg}/L may provide a better indicator than the D_{max}/L of the relationships between length, amplitude and strain.

7. Conclusions and discussion

The field-based measurements of the length, the displacement and the amplitude of the stylolites presented here demonstrate for the first time, that the amount of contractional strain accommodated by stylolites increases according to the length and the amplitude of the stylolitic topography. This finding complements and supports previous work from geochemical and petrofabric analysis (Tapp and Cook, 1988; Carrio-Schaffhausen et al., 1990), stylolite population statistics (Karcz and Scholz, 2003; Peacock and Azzam, 2006), numerical simulations of stylolite growth (Koehn et al., 2007), and mechanical considerations (Fletcher and Pollard, 1981), bearing on the interpretation of stylolites as anticracks. By implication, stylolites increase in length, amplitude, and number with increasing contractional strain in the host rock.

Although the maximum amplitude scales with stylolite length, its location along the stylolite appears random, consistent with recent work that associates maxima with processes at the grain scale, such as the positions and surface energies of less soluble grains. In contrast, the average amplitude appears related to continuum-scale factors such as rock stiffness. As a result, the maximum amplitude of stylolitic topography is not a consistent indicator of the relationships between length and strain as previously suggested (e.g. Rispoli, 1981a,b). In contrast, the average amplitude of stylolitic topography does appear to scale with the minimum magnitude of contractional strain.

Contractional strain evaluated from the measured stylolite amplitudes account for less than 20% of the visible thinning of the rock assessed independently. This implies that significant volume loss in the layer must have been accommodated by other processes, such as smaller stylolites not apparent at the outcrop scale, pressure-solution at the grain scale, or by bedding-plane slip-related dissolution. In the former case, layer thinning was probably accomplished by the earlier growth of stylolites that are sufficiently small (with length L), if compared with the average grain size l of the host rock (i.e. $L/l < 10$), to allow for dissolution and contractional strain without the development of a stylolitic topography (in agreement with Koehn et al., 2007).

Although this minimum value of 20% could be a minimum value it is consistent with results obtained by Missenard (2003), Micarelli et al. (2004) and Benedicto et al. (2004). These authors studied, at different scales, deformation occurring in the damage zones of the

La Remuque and the Blegiers normal faults, in the French Alps (Missenard, 2003; Micarelli et al., 2005), and of the Pyrgaki fault, in the Corinth rift (Benedicto et al., 2004). Their geometrical restoration of stretched and thinned micrite-limestone layers from fault zones suggests that deformation in such carbonates is accommodated at 80% by structures of brittle deformation, as open (mode I) and shear (mode II or III) fractures, and 20% by physico-chemical processes, such as pressure-solution phenomena, that reduce rock volume.

Acknowledgments

The authors are grateful to the reviewers, Jean-Pierre Gratier and Stefano Tavani, and to special issue editors Fabrizio Agosta and Emanuele Tondi, for their detailed comments that have improved the final paper. This work was supported by a Visiting Professorship at the Université de Paris-Sud, Orsay, France to RAS and by grants to RAS from NASA's Planetary Geology and Geophysics Program, which are gratefully acknowledged.

References

Aki, K., Richards, P.G., 1980. Quantitative Seismology: Theory and Methods, vol. I. W.H. Freeman, San Francisco, California.

Benedicto, A., Labaume, P., Micarelli, L., Carrio, E., 2004. Deformation mechanisms in extensional fault propagation folding involving carbonate rocks: the Pyrgaki fault, Corinth rift (Greece). In: Réunion des Sciences de la Terre, Poster Proceedings. Société Géologique de France, Strasbourg, France.

Boncio, P., Brozzetti, F., Lavecchia, G., 2000. Architecture and seismotectonics of a regional low-angle normal fault zone in Central Italy. Tectonics 19, 1038–1055.

Boschi, E., Guidoboni, E., Ferrari, G., Valensise, G., Gasperini, P., 1997. CFTI, Catalogo dei Forti Terremoti Italiani dal 461 a.C. al 1990. Istituto Nazionale di Geofisica, Storia Geofisica Ambientale, Bologna.

Bussolotto, M., Micarelli, L., Benedicto, A., Invernizzi, C., Deiana, G., 2005. Deformation features of the Gubbio fault zone. Rendiconti Società Geologica Italiana 1, 61–62.

Bussolotto, M., Micarelli, L., Benedicto, A., Invernizzi, C., Deiana, G., 2007. Deformation features within an active normal fault zone in carbonate rocks: the Gubbio fault (Central Apennines, Italy). Journal of Structural Geology 29 (12), 2017–2027.

Brouste, A., Renard, F., Gratier, J.P., Schmittbuhl, J., 2007. Variety of stylolites' morphologies and statistical characterization of the amount of heterogeneities in the rock. Journal of Structural Geology 29, 422–434.

Carrio-Schaffhausen, E., Raynaud, S., Latiere, H., Mazerolles, F., 1990. Propagation and localization of stylolites in limestones. In: Jones, M., Preston, R. (Eds.), Deformation Mechanisms: Rheology and Tectonics. Geological Society of London, Special Publication, vol. 54, pp. 193–199.

Clark, R.M., Cox, S.J.D., 1996. A modern regression approach to determining fault displacement–length relationships. Journal of Structural Geology 18, 147–152.

Collettini, C., Barchi, M.R., Chiaraluce, L., Mirabella, F., Pucci, S., 2003. The Gubbio fault: can different methods give pictures of the same object? Journal of Geodynamics 36, 51–66.

Fletcher, R.C., Pollard, D.D., 1981. Anticrack model for pressure solution surfaces. Geology 9, 419–424.

Holcomb, D., Rudnicki, J.W., Issen, K.A., Sternlof, K., 2007. Compaction localization in the Earth and the laboratory: state of the research and research directions. Acta Geotechnica 2, 1–15.

Karcz, Z., Scholz, C.H., 2003. The fractal geometry of some stylolites from the Calcare Massiccio Formation, Italy. Journal of Structural Geology 25, 1301–1316.

Katsman, R., Aharonov, E., 2006. A study of compaction bands originating from cracks, notches and compacted defects. Journal of Structural Geology 28, 508–518.

Katsman, R., Aharonov, E., Scher, H., 2006. Localized compaction in rocks: Eshelby's inclusion and the spring network model. Geophysical Research Letters 33, L10311. doi:10.1029/2005GL025628.

Koehn, D., Renard, F., Toussaint, R., Passchier, C.W., 2007. Growth of stylolite teeth patterns depending on normal stress and finite compaction. Earth and Planetary Science Letters 257, 582–595.

Kostrov, B., 1974. Seismic moment and energy of earthquakes, and seismic flow of rock. Izvestiya Physics of the Solid Earth 13, 13–21.

Menichetti, M., Minelli, G., 1991. Extensional tectonics and seismogenesis in Umbria (Central Italy). The Gubbio area. Bollettino della Società Geologica Italiana 110, 857–880.

Micarelli, L., Benedicto, A., Saint-Bezar, B., Vergély, P., 2004. Zones de faille en domaîne carbonaté. Final Project Report, Total-UPSXI, p. 118, unpublished.

Micarelli, L., Benedicto, A., Invernizzi, C., Saint-Bezar, B., Michelot, J.L., Vergély, P., 2005. Influence of *P*/*T* conditions on the style of normal fault initiation and growth in limestones from the SE-Basin, France. Journal of Structural Geology 27, 1557–1598.

Missenard, Y., 2003. Quantification des mécanismes de la déformation cassante en domaine carbonaté: Cas des failles normales du Tithonique du bassin du Sud-Est, France. Mémoire de DEA., Université Paris XI, Orsay, France, p. 40.

Mollema, P.N., Antonellini, M.A., 1996. Compaction bands: a structural analog for anti-mode I cracks in eolian sandstone. Tectonophysics 267, 209–228.

Molnar, P., 1983. Average regional strain due to slip on numerous faults of different orientations. Journal of Geophysical Research 88, 6430–6432.

Olson, J.E., 2003. Sublinear scaling of fracture aperture versus length: an exception or the rule? Journal of Geophysical Research 108, 2413. doi:10.1029/2001JB000419.

Passchier, C.W., Trouw, R.A.J., 1996. Microtectonics. Springer, New York, p. 289.

Peacock, D.C.P., Azzam, I.N., 2006. Development and scaling relationships of a stylolite population. Journal of Structural Geology 28, 1883–1889.

Petit, J.P., Mattauer, M., 1995. Palaeostress superimposition deduced from mesoscale structures in limestone: the Matelles exposure, Languedoc, France. Journal of Structural Geology 17, 245–256.

Renard, F., Dysthe, D., 2003. Pressure solution. In: Middleton, G.V. (Ed.), Encyclopedia of Sediments and Sedimentary Rocks. Kluwer, pp. 542–543.

Renard, F., Schmittbuhl, J., Gratier, J.P., Meakin, P., Merino, E., 2004. Three-dimensional roughness of stylolites in limestones. Journal of Geophysical Research 109, B03209. doi:10.1029/2003JB002555.

Rispoli, R., 1981a. Microtectonique et champ de constraints dans les calcaires fins du Languedoc, exemple des matelles et du cirque de Navacelles. Ph.D. thesis, Université des Sciences et Techniques du Languedoc, Montpellier, France, p. 93.

Rispoli, R., 1981b. Stress fields about strike-slip faults inferred from stylolites and tension gashes. Tectonophysics 75, 29–36.

Rutter, E.H., 1983. Pressure solution in nature, theory and experiment. Journal of the Geological Society of London 140, 725–740.

Scholz, C.H., 1997. Earthquake and fault populations and the calculation of brittle strain. Geowissenschaften 15, 124–130.

Scholz, C.H., 2002. The Mechanics of Earthquakes and Faulting. Cambridge University Press, Cambridge, p. 471.

Scholz, C.H., Cowie, P.A., 1990. Determination of total strain from faulting using slip measurements. Nature 346, 837–838.

Schultz, R.A., 2003. Seismotectonics of the Amenthes Rupes thrust fault population. Mars, Geophysical Research Letters 30, 1303. doi:10.1029/2002GL016475.

Schultz, R.A., Soliva, R., Fossen, H., Okubo, C.H., Reeves, D.M., 2008. Dependence of displacement-length scaling relations for fractures and deformation bands on the volumetric changes across them. Journal of Structural Geology 30, 1405–1411.

Schultz, R.A., 2009. Scaling and paleodepth of compaction bands, Nevada and Utah. Journal of Geophysical Research 114, B03407. doi:10.1029/2008JB005876.

Stel, H., De Ruig, M.J., 1989. Opposite vergence of a kink fold and pressure solution cleavage, Southeast Spain: a study of the relation between paleostress and fold kinematics. Tectonophysics 165, 117–124.

Sternlof, K., Rudnicki, J.W., Pollard, D.D., 2005. Anticrack-inclusion model for compaction bands in sandstone. Journal of Geophysical Research 110, B11463. doi:10.1029/2005JB0037664.

Suppe, J., 1985. Principles of Structural Geology. Prentice-Hall, New Jersey, p. 537.

Tapp, B., Cook, J., 1988. Pressure solution zone propagation in naturally deformed carbonate rocks. Geology 16, 182–185.

Westaway, R., 1992. Seismic moment summation for historical earthquakes in Italy: tectonic implications. Journal of Geophysical Research 97, 15437–15464.

Wilkins, S.J., Schultz, R.A., Anderson, R.C., Dohm, J.M., Dawers, N.C., 2002. Deformation rates from faulting at the Tempe Terra extensional province. Mars, Geophysical Research Letters 29, 1884. doi:10.1029/2002GL015391.